Experimental and theoretical study of the fluorescence emission of ferulic acid: Possible insights into the fluorescence properties of humic substances

Experimental and theoretical study of the fluorescence emission of ferulic acid: Possible insights into the fluorescence properties of humic substances

Giovanni Ghigo, Davide Vione*, Silvia Berto*

Department of Chemistry, University of Torino, Via Pietro Giuria 5,7, 1015 Torino, Italy.

* Address correspondence to either author: *davide.vione@unito.it*; *silvia.berto@unito.it*

Abstract

Ferulic acid ((E)-3-(4-hydroxy-3-methoxy-phenyl)prop-2-enoic acid, hereinafter FA) is a building block of plant cell walls that is commonly found in lignocellulose. As such, it is a potential component of humic substances produced by microbial degradation of plant spoils. The fluorescence excitation-emission matrix spectra of FA have an interesting humic-like shape, with bands that can be assimilated to the A and C regions of humic substances. For all of these reasons, the study of FA photoluminescence might provide interesting insight into the still unknown processes that lay behind the fluorescence properties of humic compounds. FA is a weak diprotic acid that occurs in three different forms in aqueous solution (neutral H_2FA, singly deprotonated HFA^- and doubly deprotonated FA^{2-}), which have slightly different absorption and emission properties. The "A-like" fluorescence emission of the FA species is accounted for by excitation from the ground singlet state S_0 to singlet excited states higher than the first (S_4 for H_2FA, S_5 for HFA^-, and a state higher than S_2 for FA^{2-}), followed by radiationless deactivation to the first excited singlet state (S_1) and fluorescence emission according to the $S_1 \rightarrow S_0$ transition. In contrast, the "C-like" emission is mainly caused by $S_0 \rightarrow S_1$ excitation combined with $S_1 \rightarrow S_0$ emission, but there is also a minor contribution from the $S_0 \rightarrow S_2$ excitation that becomes significant for HFA^-. The uneven variations with pH of the wavelengths of the maximum FA radiation absorption and fluorescence emission can be rationalised in the framework of the energy levels of the frontier (HOMO and LUMO) molecular orbitals of the different FA species. These levels are affected by charge interaction between the relevant electrons and the neutral (protonated) or negative (deprotonated) groups of each species.

Keywords: Ferulic acid; Humic substances; Fluorescence; EEM spectra; Absorption spectra; TD-DFT; Frontier molecular orbitals.

1. Introduction

Humic substances (HS) are organic matter components that make up an important fraction of the organic carbon in soil and are also key constituents of the chromophoric dissolved organic matter (CDOM) that occurs in surface waters [**1,2**]. Moreover, compounds that share some features with HS are also found as humic-like substances (HULIS) in atmospheric aerosols [**3**]. HS derive from the decomposition of organism spoils (mostly vegetal) via breaking of biological polymers such as cellulose and lignin. HS can also be formed by oligomerisation of small organic molecules [**4,5**].

The characterisation of HS has taken into account their elemental composition, optical properties, fluorescence emission, functional groups (identified by, e.g., nuclear magnetic resonance and IR spectroscopy) and molecular weight [**3,6**]. In the latter case a controversy that is not yet solved has arisen, as to whether HS have a polymeric/oligomeric structure or are rather loosely bound aggregates of smaller compounds (according to some views, both hypotheses could be correct to some extent) [**7-9**].

Fluorescence spectroscopy, and particularly that based on excitation-emission matrices (EEM), is one of the most widely used techniques for the detection of HS in water and soil samples [**10**]. EEM spectroscopy combines sensitivity, instrument accessibility, ease of use and limited sample manipulation requirements (for instance, natural water samples can be analysed as such or after filtration only), which accounts for its widespread use and application in the HS field [**11-13**]. The fluorescence of HS is characterised by two peaks, namely peak A (excitation at ~250 nm, emission at 400-450 nm) and peak C (excitation at ~350 nm, emission at 400-450 nm) [**14,15**]. These peaks allow HS to be easily identified in EEM spectra, but the reason of peak occurrence and the nature of the relevant fluorophores are still unknown. It is also unsure whether the behaviour of the single fluorophores can be maintained in complex HS mixtures [**16**].

Several studies have shown that substances with humic-like fluorescence can be formed from phenolic compounds, under conditions that trigger the formation of phenoxy radicals and subsequent oligomerisation pathways [**17,18**]. Interestingly, similar processes are also thought to produce secondary organic aerosol precursors, as well as atmospheric HULIS [**19,20**]. These findings are supported by the theoretical prediction that phenol oligomers with three or more aromatic rings would emit fluorescence radiation at 400-450 nm [**21**].

However, other studies have described the emission of fluorescence radiation in the humic region in the case of smaller molecules, characterised by the occurrence of aromatic rings as well as of oxygen-containing functional groups, such as -C=O and -OH. Examples include 4-hydroxybenzophenone [**22**] and gallic acid [**23**]. Moreover, a photo-oxidation process causing hydroxylation of the indole ring might possibly account for the development of humic fluorescence upon irradiation of L-tryptophan, which does not undergo photo-oligomerisation [**24**].

Ferulic acid ((E)-3-(4-hydroxy-3-methoxy-phenyl)prop-2-enoic acid) is a building block of lignocellulose, and it is commonly found in plant cell walls [**25,26**]. There is literature evidence that this compound has fluorescence emission around 400 nm [**27,28**], which overlaps with the region

where HS emit. However, to our knowledge the EEM spectra of ferulic acid have never been described or reported so far, which prevents an assessment of how much humic-like the fluorescence of this compound is. In addition, the nature of the transitions that are responsible for the fluorescence emission by ferulic acid is still unknown. This compound has potential importance as humic fluorophore, due to both its association with lignocellulose (the degradation of which is one of the HS sources) and its fluorescence emission region. Therefore, the present work has the goals of studying in detail the nature of the fluorescence emission transitions of ferulic acid, and of providing its EEM spectra at different pH values after verification of their humic-like character. The results will provide additional insight into the possible nature of humic fluorophores.

2. Materials and Methods

2.1 Chemicals

Trans-ferulic acid ((E)-3-(4-hydroxy-3-methoxy-phenyl)prop-2-enoic acid) (99%) (hereinafter FA), quinine hemisulphate salt monohydrate (99.0-101.0%), acetonitrile (gradient grade) and sulphuric acid (95% - 97%) were from Sigma Aldrich (St. Louis, Missouri, US). Suwannee River II standard Humic Acid (SRHA) wase obtained from the International Humic Substances Society. A quinine sulphate solution (4 μg L^{-1}) in 5 mmol L^{-1} H_2SO_4 was used as reference for fluorescence emission intensity. Potassium hydroxide (0.1 mol L^{-1}) and hydrochloric acid (0.1 mol L^{-1}), used for adjusting the pH of the FA solutions, were prepared by diluting Merck (Darmstadt, Germany) concentrated products. pH buffer reference solutions at pH 4.00 ± 0.02 and 7.00 ± 0.02 were from Merck. Grade-A glassware and ultra-pure water (Milli-Q, Millipore) were used to prepare all the solutions.

2.2 Instrumentation

A Jasco V-550 UV–Vis double-beam spectrophotometer, equipped with Hellma quartz cuvettes (1.000 cm optical path length) was used to record the absorption spectra. The fluorescence excitation–emission matrix (EEM) spectra were recorded with a Varian Cary Eclipse fluorescence spectrofluorometer, using a Helma quartz cuvette (1.000 cm × 1.000 cm optical path length). The pH of the solutions was measured by a Metrohm potentiometer (model 713, resolution of ±0.1 mV), equipped with a Metrohm combined glass electrode (mod. 6.0259.100). The electrode was calibrated in activity scale using pH buffer reference solutions.

2.3 Procedures

The UV–Vis spectra were recorded in the wavelength range from 200 to 500 nm, measuring absorbance each 1 nm. The baseline was taken in air before each measurement, and the absorbance spectra were taken against the reference cuvette filled with Milli-Q water. The fluorescence

excitation–emission matrix (EEM) spectra were recorded using excitation wavelengths from 200 to 500 nm and emission wavelengths from 250 to 600 nm or from 250 to 500 nm. The increment of the excitation wavelength was of 5 nm, and emission and excitation slit widths of 5 nm were used. The fluorescence emission was recorded each 1 nm. Spectrophotometric and fluorimetric measurements were performed on solutions having a FA concentration of 1.0×10^{-5} mol L^{-1}.

In some experiments, fluorescence emission spectra of 1.0×10^{-5} mol L^{-1} FA solutions were recorded at the maximum excitation wavelength of each relevant species (protonated H_2FA, partially dissociated HFA^- and fully deprotonated FA^{2-}). The fluorescence emission intensity was expressed as QSU - Quinine Sulphate Units (fluorescence emission of a 1 µg L^{-1} solution of quinine sulphate in 5 mmol L^{-1} H_2SO_4, at $\lambda_{ex}/\lambda_{em}$ 350/450 nm) [**29**]. The emission spectra of the quinine sulphate reference solutions were recorded in triplicate for each measurement session, in the wavelength range 360 – 550 nm, using an excitation wavelength of 350 nm and emission/excitation slit widths of 10 nm. Then, the emission intensities of the FA solutions were divided for the quinine sulphate emission at 450 nm, so as to remove the signal fluctuations due to instrumental conditions.

2.4 Computational Methods

The computational study was performed within the Density Functional Theory (DFT) [**30-32**]. Bulk solvent effects to the electronic energies were introduced in all calculations by the universal Solvation Model Density [**33,34**].

The absorption spectra were obtained with single-point Time-Dependent DFT (TD-DFT)[**35,36**], by carrying out calculations on the geometries of neutral and dissociated FA. This method provides a reasonable accuracy at reasonable computational costs (time and computing resources) [**37-39**]. While the excitation energies calculated in this way correspond to the maxima in the absorption spectra, this approach does not include vibrational contributions or dynamic solvent effects. For the FA neutral species, the best agreement with the experimental findings was obtained without explicit water molecules (H_2FA). For the two dissociated anionic species that can occur in aqueous solvent, some explicit water molecules were required to predict the absorption maxima well: the mono-dissociated anion required four explicit water molecules localized around the carboxylate group ($[HFA\ (H_2O)_4]^-$); the doubly dissociated dianion required two other water molecules localized around the oxyl group ($[FA\ (H_2O)_6]^{2-}$).

The geometry of each species was re-optimised in its first excited singlet state. Because electronic transitions are much faster than molecular geometry modifications [**40**], the difference between the energies of the first excited states and those calculated for the ground states at the excited state geometries was taken as emission (fluorescence) energy. In these calculations, all three species were optimised with six explicit water molecules (four localized around the carboxylic group and two around the para-hydroxyl group). For computations we used the functional PBE0 [**41-43**], in combination with the Pople's basis set 6-311+G(d,p) [**44,45**].

The exact calculation of the pK_a of an acid is quite a though challenge [**46**]. Here, the deprotonation equilibria were modelled with the same fruitful approach used in previous works [**22,23**], which allowed for getting good agreement between the calculated and experimental pK_a values. The method consisted in the calculation of the free energy of proton transfer from a complex of the acid HA with six molecules of water, to a tetramer of water:

$$[HA\ (H_2O)_6] + (H_2O)_4 \leftrightarrows [A\ (H_2O)_6]^- + [H_3O\ (H_2O)_3]^+ \qquad (1)$$

All calculations were performed using the quantum package Gaussian 09-A [**47**]. The pictures of the structures in **Figure 2** and in **Figures S3–S5, S8** in the Supplementary Material (hereinafter SM) were obtained with the graphical program Molden [**48**].

3. Results and Discussion

3.1. Absorption spectra

The UV-visible spectra recorded on FA solutions as a function of pH show that the position and the molar absorptivity of the absorption maxima appreciably change with the protonation level of the molecule, which is a weak diprotic acid. The reported protonation constants of FA (pK_a values) are 4.50 and 8.92 (I = 0.10 mol L^{-1}, T = 25°C) [**49**], or 4.70 and 9.32 at I = 0 mol L^{-1} and T = 25°C (values calculated from the experimental ones, upon application of an extended Debye-Hückel equation [**50**]). These values are quite well reproduced by our calculations: we estimated computationally pK_{a1} = 5.6 and pK_{a2} = 8.9, respectively (see **Table S1** in the SM). On this basis, the species distribution diagram (reported in **Figure S1** of the SM) shows that a single FA species strongly prevails over the others in solution at pH 2 (H_2FA), pH 6.5 (HFA^-), and pH 11 (FA^{2-}). For this reason, the experimental absorption spectra were measured at the mentioned pH values and they are shown in **Figure 1**.

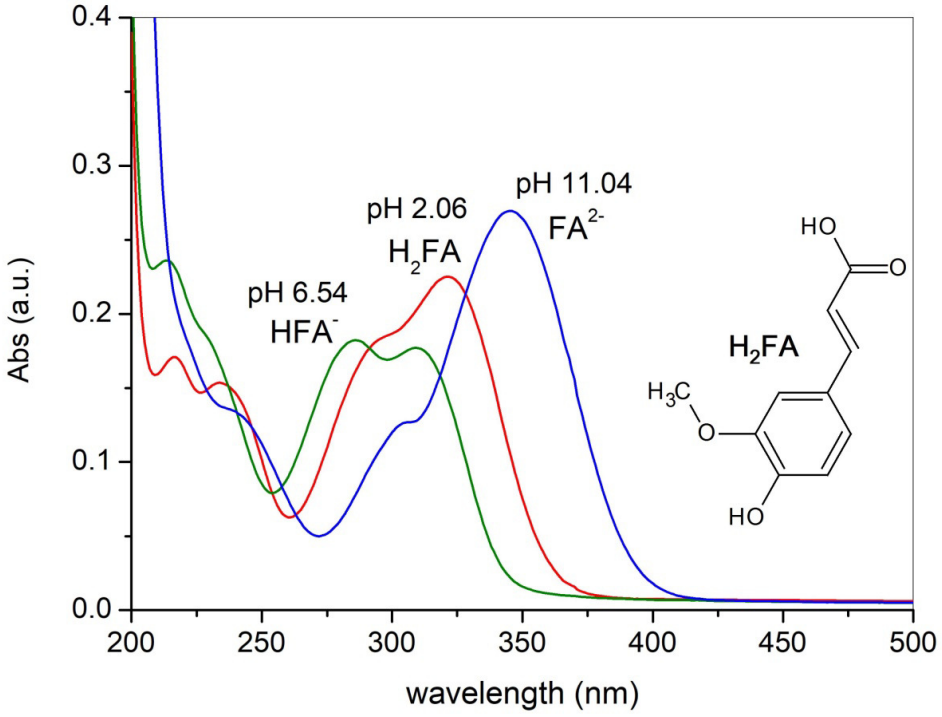

Figure 1. Experimental absorption spectra of a solution of ferulic acid 1×10^{-5} mol L^{-1} at different pH values. The structure of the protonated species H_2FA is also reported. The groups undergoing deprotonation are the carboxylic and the phenolic ones.

At pH 2 the neutral form of FA (H_2FA in **Figure 1**) shows four absorption maxima at 321, ~295, 235, and 217 nm. The first deprotonation (pH 6.5), which involves the carboxylic group, causes a shift in the absorption maxima towards shorter wavelengths: 309, 286, ~228, and 214 nm, respectively (see HFA^- in **Figure 1**). In contrast, further deprotonation of the phenolic group to give the dianionic form (pH 11) shifts the maxima at longer wavelengths: respectively, 345, 305, ~242, and ~223 nm (see FA^{2-} in **Figure 1**). The four absorption maxima of H_2FA are quite well reproduced by the theory: the transitions we calculated at 332 ($S_0 \rightarrow S_1$), 290 ($S_0 \rightarrow S_2$), 240 ($S_0 \rightarrow S_4$), and 216 nm ($S_0 \rightarrow S_6$) have to be compared, respectively, with the experimental data obtained at 321, 295, 235, and 217 nm. The calculations indicate that the excitations to states S_3 and S_5 are too weak to be registered in the absorption spectrum (see oscillator strengths *f* in **Table S2** of the SM). Reasonable calculation accuracy for the charged species (HFA^-, FA^{2-}) could only be obtained for the first two or three absorption maxima. For HFA^- we calculated 314 ($S_0 \rightarrow S_1$), 275 ($S_0 \rightarrow S_2$), and 239 nm ($S_0 \rightarrow S_4$), to be compared with the respective experimental values of 309, 286 and 228 nm (the latter is a shoulder peak). For FA^{2-} we calculated 354 ($S_0 \rightarrow S_1$) and 282 nm ($S_0 \rightarrow S_2$), compared to the experimental data at, respectively, 345 and 305 nm. Almost all calculated values were within 10 nm of each corresponding experimental value. A simulation of the absorption spectra, based on the computational results, is reported in **Figure S2** in the SM.

Both experimental data and theoretical computations suggest the occurrence of intense transitions above 300 nm. These are the longer-wavelength transitions for the three FA species, and calculations suggest that they are of the kind $S_0 \rightarrow S_1$. **Figure 2** reports the differential electronic density maps, which graphically show the changes occurring in the electronic densities when the molecules go from the ground state S_0 to the first excited state S_1. These maps show that, for all three species (H_2FA, $[HFA(H_2O)_4]^-$, and $[FA(H_2O)_6]^{2-}$), the transitions to S_1 are characterized by an electron transfer from the phenyl ring, the hydroxyl and methoxyl groups toward the carboxy-vinyl moiety (CH=CH-COO(H)).

The calculations indicate that the most important component in the $S_0 \rightarrow S_1$ transitions (weight of 96-98%, see **Table S2** in the SM) is the promotion of one electron from the highest occupied molecular orbital (HOMO) to the lowest unoccupied molecular orbital (LUMO, see **Figure S3** in the SM). In all three cases (H_2FA, HFA^- and FA^{2-}) the HOMOs correspond to combinations of the lone-pair *p* orbitals of the methoxyl and hydroxyl groups with a π orbital of the benzene ring. The LUMOs correspond to combinations of the π_{CC}^* orbital of the ethendiyl moiety with the π_{CO}^* orbital of the carboxyl group, plus some contribution by a π^* orbital of the benzene ring. The energies of these orbitals are graphically shown in **Figure 3**. The HOMO-LUMO transition in H_2FA requires 4.28 eV. This is quite different from 3.73 eV for the transition calculated at 332 nm (and observed at 321 nm) because the HOMO-LUMO transition, although dominant in $S_0 \rightarrow S_1$, is not its only component. Therefore, an exact correspondence in the transition energies cannot be expected.

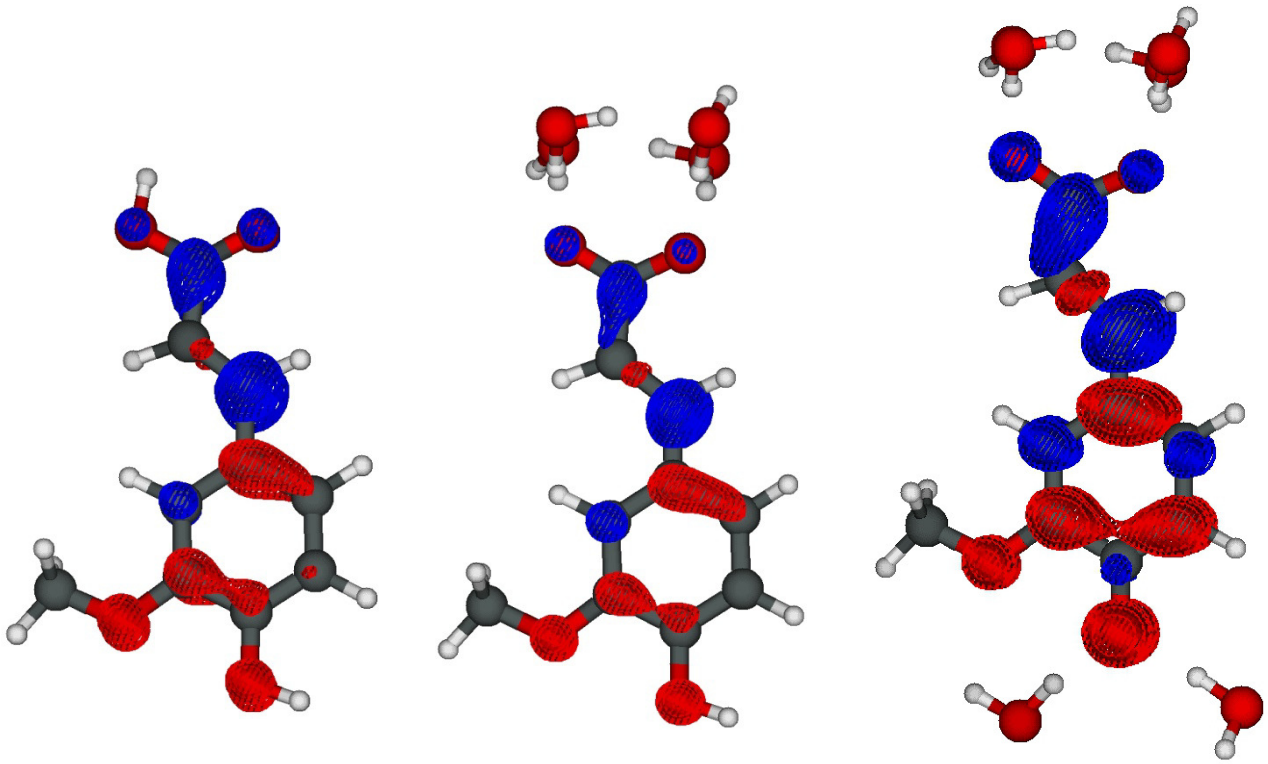

Figure 2. Differential electronic density maps for the first excited states (S_1) of H_2FA (left), $[HFA(H_2O)_4]^-$ (center) and $[FA(H_2O)_6]^{2-}$ (right), with respect to S_0. The red areas correspond to a reduction in the electronic density when going from S_0 to S_1, and the blue areas correspond to an increase in the electronic density.

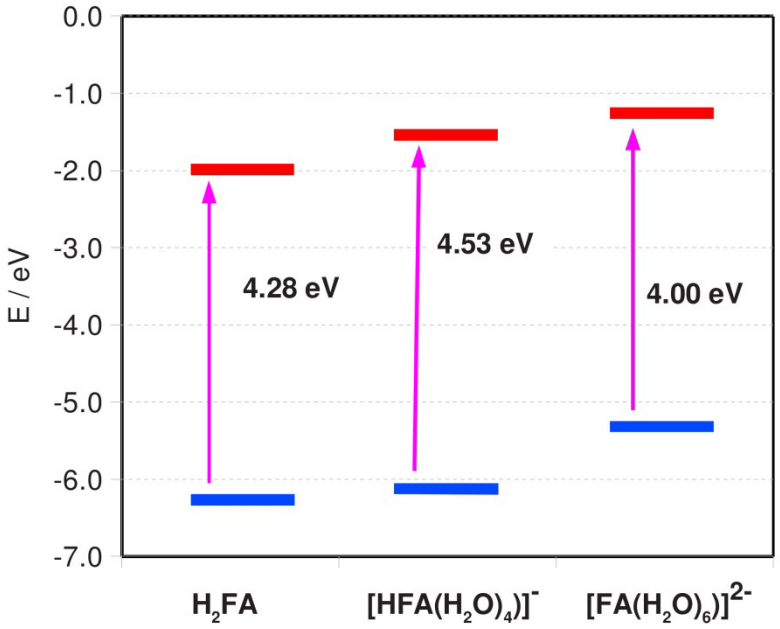

Figure 3. Electronic energies of the HOMOs (blue segments) and of the LUMOs (red segments) of H_2FA, $[HFA(H_2O)_4]^-$, and $[FA(H_2O)_6]^{2-}$.

A more detailed discussion of the HOMO-LUMO transitions of the three FA species can explain why the wavelength of maximum absorption by HFA^- is shorter compared to H_2FA (hypsochromic shift), while in the case of the absorption maximum of FA^{2-} one has longer wavelength compared to H_2FA (bathochromic shift). By comparing $[HFA(H_2O)_4]^-$ with H_2FA, one can observe that the energy of the LUMO raises (+0.41 eV) in the case of $[HFA(H_2O)_4]^-$. The reason is electron repulsion, because this orbital is mainly localized in the negatively charged CH=CH-COO^- moiety (see **Figure S4** in the SM). In contrast, the energy of the HOMO is hardly affected by deprotonation (+0.16 eV for $[HFA(H_2O)_4]^-$ compared to H_2FA), because the HOMO is not directly involved in the delocalisation of the negative charge. The overall consequence is an increase of 0.25 eV in the HOMO-LUMO gap (reaching 4.53 eV in the case of $[HFA(H_2O)_4]^-$), which causes the hypsochromic shift. In the case of $[FA(H_2O)_6]^{2-}$, one can observe that the double negative charge further increases the energy of the LUMO (+0.27 eV). However, the energy of the HOMO is increased even more (+0.80 eV), because it includes a large contribution by the phenoxyl anion. The result is a reduction by 0.53 eV of the energy of the HOMO-LUMO gap for $[FA(H_2O)_6]^{2-}$ (now at 4.00 eV) compared to $[HFA(H_2O)_4]^-$, and a reduction by 0.28 eV compared to H_2FA, which accounts for the observed bathochromic shift.

The second excited states also show a partial character of electron transfer (see **Figure S5** in the SM) from the phenyl ring, the hydroxyl and methoxyl groups toward the carboxy-vinyl moiety (CH=CH-COO(H)). However, their multi-configurational nature (see **Table S2** in the SM) prevents a simple analysis to be carried out based on the molecular orbitals.

An important issue to be underlined is that, differently from the fluorescence spectra (*vide infra*), the absorption spectra of FA are definitely not humic-like at any pH value. Actually, the absorption spectra of humic substances show a featureless exponential decay with increasing wavelength [**3,5,8**], which is very different from the molecular-band structure of the FA spectrum. The real nature of the humic absorption spectra seemed to be elegantly elucidated some years ago by assuming inter-molecular interactions [**51**], instead of hypothesising definite (but never isolated or identified) chromophores or the (very hard to demonstrate) envelope of multiple absorption spectra. However, recent evidence has strongly questioned the interaction hypothesis [**52**], thus the quest for the actual humic chromophores (which might even be single compounds, although this is far from certain) should start back almost from scratch. Still, there is no compelling reason to believe that humic chromophores and fluorophores should be the same. The case of proteins is particularly illuminating in this sense: protein-like fluorescence is mostly accounted for by tyrosine and tryptophan that, however, are not the only light-absorbing amino-acids. The radiation energy absorbed by proteins is channelled towards the two amino-acidic fluorophores [**53**], and the same might happen with humic compounds. Therefore, the non-humic absorption of FA would not impair its potential role as model for humic fluorophores, although the present results show that it is certainly not a model for humic chromophores. With these premises, it should be underlined that there is no assurance at all that the quest for a single molecule showing both humic absorption and humic fluorescence may meet with any success.

3.2. Fluorescence spectra

The fluorescence EEM spectra recorded on solutions containing 1×10^{-5} mol L^{-1} FA at different pH values are shown in **Figure 4**. Interestingly, these spectra show peaks that are located in the A and C regions of humic substances, with emission wavelengths that range at 400-450 nm depending on pH. This humic-like feature of FA fluorescence in water is not so common, which should be stressed. For instance, 4-hydroxybenzophenone (4OHBP) in aprotic organic solvents shows an emission band that overlaps with peak C, but it definitely lacks peak A. Moreover, 4OHBP fluorescence is effectively quenched in aqueous solution [**54**]. Fluorescence emission by protonated (neutral) gallic acid is centred at 350 nm, and is thus outside of the humic region. Only deprotonated (anionic) gallic acid shows peaks that can be assimilated to the humic A and C emissions [**23**]. Finally, typically biomass-burning compounds such as o-vanillin, vanillic acid, syringol and acetosyringone have similar emission properties as neutral gallic acid. The appearance of humic-like fluorescence has only been observed from irradiated o-vanillin and acetosyringone, under conditions that trigger oligomerisation because of the involvement of phenoxyl dimerisation and/or Norrish-type reactions. Interestingly, in that case the appearance of humic fluorescence was closely connected to the occurrence of oligomeric species and not to the original compounds [**55**].

For the above reasons, the fact that FA shows fluorescence peaks that are similar to peak A and peak C of humic substances at practically all pH values in aqueous solution deserves investigation. The protonated FA molecule (H_2FA, pH 2.0) shows an asymmetric peak at excitation/emission wavelengths ($\lambda_{Ex/Em}$) of 321/460 nm, and a second less intense peak at $\lambda_{Ex/Em}$ = 240/460 nm. These two peaks correspond to two different excitations from S_0 to, respectively, the S_1 and S_4 states of H_2FA (coherently with the 321 and 235 nm maxima in the absorption spectrum), combined to a unique emission from S_1 that follows Kasha's rule [**56**] and is calculated at 422 nm (oscillator strength, f = 1.08). The discrepancy of ~40 nm between the calculated and experimental values of the emission wavelength is due to the vibrational component, which is very important in the fluorescence phenomena but is not taken into account in our calculations.

The monoanionic species (HFA^-, pH 6.5) shows two nearby emission maxima at $\lambda_{Ex/Em}$ = 310/415 and 290/415 nm, and a secondary peak at $\lambda_{Ex/Em}$ = 230/419 nm. These three peaks correspond to excitations from S_0 to the S_1, S_2 and S_5 states (respectively corresponding to the 309, 286, and 228 nm maxima in the absorption spectrum), and to an emission from the S_1 state (calculated at 401 nm, f = 1.12).

Finally, the dianionic species (FA^{2-}, pH 10.0) has an emission maximum at $\lambda_{Ex/Em}$ = 347/469 nm and a minor peak at $\lambda_{Ex/Em}$ = 245/470 nm that correspond, respectively, to the 345 and 242 nm maxima in the absorption spectrum. Both emissions are from the state S_1 (calculated at 439 nm, f = 1.26), with the first corresponding to a $S_0 \rightarrow S_1$ excitation followed by $S_1 \rightarrow S_0$ emission, while in the second case the excitation is of the kind $S_0 \rightarrow S_n$, with n possibly higher than 2. However, this latter transition is not well reproduced by the calculations.

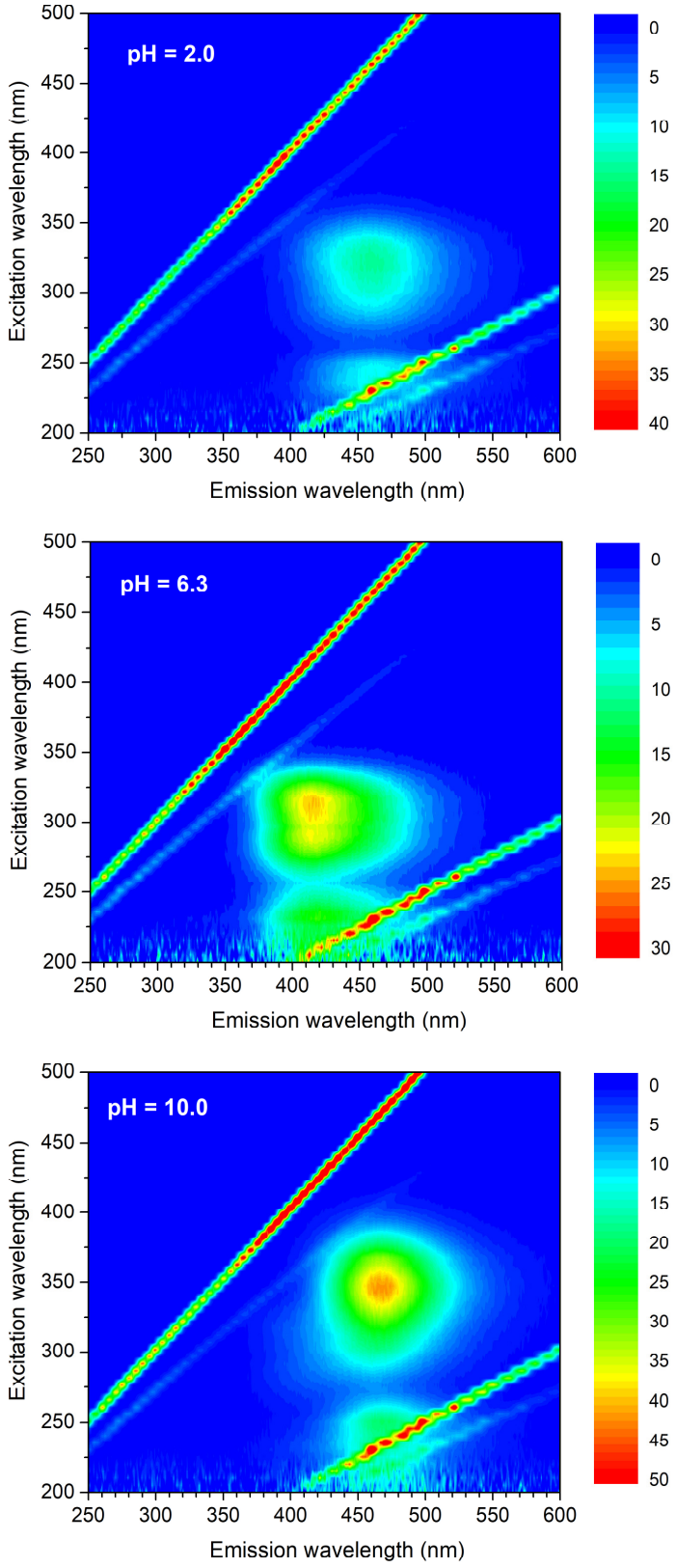

Figure 4. Fluorescence EEMs of a solution of ferulic acid (1×10^{-5} mol L^{-1}) at three different pH values, where the prevailing species are H_2FA (pH 2.0), HFA^- (pH 6.3) and FA^{2-} (pH 10.0). Emission intensities are expressed as arbitrary units.

Despite the limits in the accuracy with which the emission wavelengths are predicted, the calculations reproduce qualitatively well their variations as a function of pH (the experimental emission wavelengths follow in fact the order HFA^- < H_2FA < FA^{2-}). In a similar way as for the excitation wavelengths (in particular, those related to the $S_0 \rightarrow S_1$ transitions), the emission wavelengths ($S_1 \rightarrow S_0$) are coherent with the variations of the HOMO-LUMO gap of the three different FA species. The trend can thus be semi-quantitatively interpreted with variations in the HOMO and/or LUMO energy as a function of the deprotonation process. The calculated shifts of ca. 50-90 nm between the $S_0 \rightarrow S_1$ (absorption) and $S_1 \rightarrow S_0$ (emission) transitions, which are here predicted even when neglecting the vibrational (Stokes-shift) effects, are due to changes in the structures of the excited states with respect to those of the ground states (see **Figure S6** in the SM for details). Indeed, while $S_0 \rightarrow S_1$ is calculated with the ground-state (S_0) geometry, calculations for $S_1 \rightarrow S_0$ are based on the geometry of S_1.

An interesting issue derived from DFT calculations is that the excited S_1 state of H_2FA is a rather strong acid, with a pK_a value estimated at around 1.0 (see **Table S1** and **Figure S7**, both in the SM). Indeed, H_2FA-S_1 is a much stronger acid than ground-state H_2FA (H_2FA-S_0, with pK_a = 4-5). Interestingly, a quite similar finding has been obtained previously in the case of 4-hydroxybenzophenone, with the calculated pK_a value dropping from 8.3 for S_0, down to -0.9 for S_1 [**22**]. These results mean that the S_1 states can undergo deprotonation at pH values where the S_0 states are protonated, which might have important implications for the fluorescence emission process. Indeed, fluorescence emission by H_2FA might follow two alternative routes: *(i)* H_2FA-S_0 is excited to H_2FA-S_1, which gets deprotonated to HFA^--S_1 that emits fluorescence. The same HFA^--S_1 species would emit fluorescence at higher pH values, when excitation involves HFA^--S_0. Because H_2FA-S_1 deprotonation would consistently take place at pH > 1, and fluorescence emission consistently involve HFA^--S_1, the FA fluorescence signal should not change much with pH.

(ii) H_2FA-S_0 is excited to H_2FA-S_1, and the fluorescence emission takes place from H_2FA-S_1, in competition with deprotonation of H_2FA-S_1 to HFA^--S_0. This deprotonation/deactivation process has for instance been observed with 4-hydroxybenzophenone. In this framework, when increasing the solution pH, the ground-state species gradually becomes HFA^--S_0 that is excited to HFA^--S_1, from which fluorescence emission takes place. Because two species (H_2FA-S_1 and HFA^--S_1) emit fluorescence radiation at different pH values, the FA fluorescence emission should change with pH.

Figure 5 reports the FA emission spectra as a function of pH, for excitation wavelengths of 310 nm (**5a**), 325 nm (**5b**), and 345 nm (**5c**). In the first two cases the fluorescence emission wavelength was shifted, from 458 nm at pH 2-3, down to 416 nm at pH > 4. This finding can only be explained if fluorescence emission takes place from H_2FA-S_1 at the more acidic pH values, and from HFA^--S_1 under less acidic conditions. The fluorescence signal actually reflects an acid-base equilibrium centred at pH ~4, thereby involving H_2FA-S_0 ⇆ HFA^--S_0 + H^+ rather than H_2FA-S_1 ⇆ HFA^--S_1 + H^+. Finally, excitation at 345 nm mainly involves FA^{2-}-S_0 that is promoted to FA^{2-}-S_1, from which fluorescence emission at 466 nm takes place (**Figure 5c**). The emission intensity increases with increasing pH, in analogy with the pH behaviour of the FA^{2-}-S_0 molar fraction.

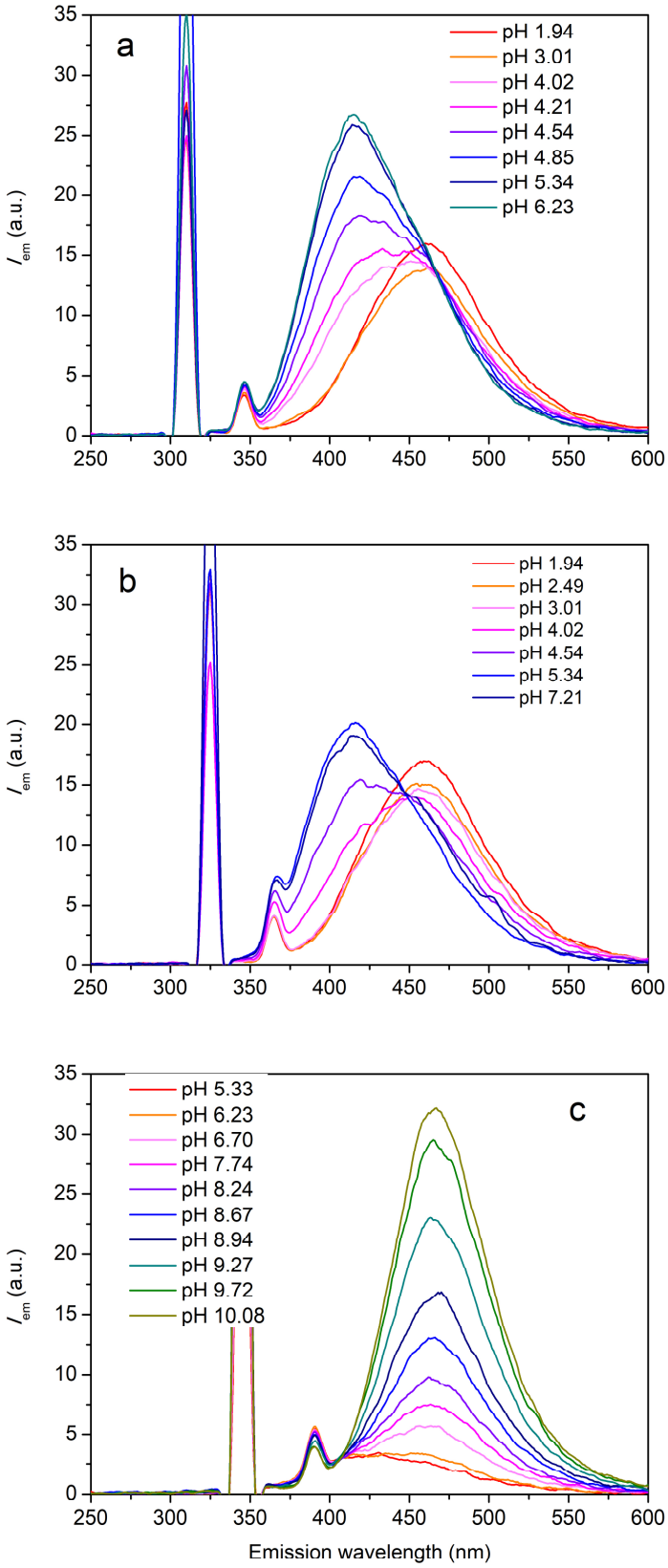

Figure 5. Fluorescence emission spectra of 1×10^{-5} mol L^{-1} FA at different pH values, for excitation wavelengths of: **(a)** 310 nm; **(b)** 325 nm, and **(c)** 345 nm.

Therefore, the dynamics of the FA ground and excited states, including the fluorescence emission processes (highlighted below in bold style) can be depicted as follows (note that our experimental data are silent as to the possible deprotonation of HFA^{-}-S_1):

$H_2FA\text{-}S_0 \leftrightarrows HFA^{-}\text{-}S_0 + H^{+}$ (2)

$HFA^{-}\text{-}S_0 \leftrightarrows FA^{2-}\text{-}S_0 + H^{+}$ (3)

$H_2FA\text{-}S_0 + h\nu \rightarrow H_2FA\text{-}S_1$ (4)

$H_2FA\text{-}S_1 \rightarrow H_2FA\text{-}S_0 + h\nu'$ **(5)**

$H_2FA\text{-}S_1 \leftrightarrows HFA^{-}\text{-}S_0 + H^{+}$ (6)

$HFA^{-}\text{-}S_0 + h\nu \rightarrow HFA^{-}\text{-}S_1$ (7)

$HFA^{-}\text{-}S_1 \rightarrow HFA^{-}\text{-}S_0 + h\nu''$ **(8)**

$FA^{2-}\text{-}S_0 + h\nu \rightarrow FA^{2-}\text{-}S_1$ (9)

$FA^{2-}\text{-}S_1 \rightarrow \rightarrow FA^{2-}\text{-}S_0 + h\nu'''$ **(10)**

Finally, it is interesting to compare the fluorescence emission of FA to that of actual humic acids (represented by the SRHA sample under study). The EEM spectra of SRHA are reported in **Figure S8** (SM), for three different pH values. Compared to the EEM spectra of FA (**Figure 4**), one notices similar excitation/emission bands. However, while the FA band position changes with pH, the same is not evident with SRHA. This difference can have two explanations: *(i)* FA is not the only SRHA fluorophore, which may be reasonable given the expected fluorescence emission of, e.g., phenol oligomers that should not undergo deprotonation like FA, and/or, *(ii)* FA in humic substances is at least partially confined into a waterless, hydrophobic environment, where acid-base equilibria cannot be operational. Moreover, the occurrence of FA in different environments might cause a band-broadening phenomenon, which would not aid the detection of pH shifts in the emission wavelengths [**57**].

It is also interesting to compare the excitation spectra of both FA and SRHA which, apart for the different pH behaviour, showed interesting similarities in the 300-350 nm signal (see **Figure S9** in SM). This finding suggest that, although the FA absorption spectrum is not humic-like, the transitions accounting for FA fluorescence might have close analogies with those involved in humic fluorescence.

4. Conclusions

The fluorescence spectrum of ferulic acid has a humic-like shape, and the emission peaks at 400-500 nm (the exact values of the emission wavelengths vary with pH, depending on the prevailing species H_2FA, HFA^{-} or FA^{2-}) fall within the A and C regions of humic substances. In particular, the ferulic acid signals with excitation wavelengths centred at 220 nm overlap with humic peak A. The fluorescence of ferulic acid in this region is due to excitation from the ground state S_0 to the excited

states S_4 in H_2FA, S_5 in HFA^-, and to an excited state higher than S_2 in FA^{2-}, followed by radiationless deactivation down to S_1 and fluorescence emission following the transition $S_1 \rightarrow S_0$. The other ferulic acid signals have excitation wavelengths in the range of 300-350 nm, depending on pH, and overlap with peak C of humic substances. In this case the excitation follows the $S_0 \rightarrow S_1$ transition, with a secondary contribution from $S_0 \rightarrow S_2$ that becomes significant in the case of HFA^-. It follows radiationless deactivation to S_1 (when relevant), and fluorescence emission according to the $S_1 \rightarrow S_0$ transition. These findings shed light on the nature of the transitions involving a fluorophore (FA) that shows interesting analogies with humic fluorophores (most notably, EEM spectra and bands in excitation spectra). The fact that the pH trend of FA fluorescence is not reflected in a similar trend of model humic substances, might possibly reflect the environment (waterless hydrophobic cores?) in which the humic fluorophores could at least in part be located.

The variation with pH of the emission wavelengths of the different species of ferulic acid (λ_{Em} follows the order $HFA^- < H_2FA < FA^{2-}$) can be accounted for when considering the energies of the HOMO and LUMO orbitals (HOMO-LUMO transitions account indeed for a good fraction of $S_0 \rightarrow S_1$, and vice versa for the emission, although the two phenomena do not fully overlap). Compared to H_2FA, the HOMO and LUMO energies are higher in the case of the deprotonated species due to electrostatic repulsion. However, in the case of HFA^- it is the LUMO that is mostly destabilised, with an increase in the gap energy and a decrease in λ_{Em} (hypsochromic shift). In contrast, in the case of FA^{2-} the destabilisation mostly involves the HOMO, and it causes the gap energy to decrease and λ_{Em} to increase (bathochromic shift).

Differently from fluorescence, the absorption spectra of ferulic acid have no humic-like characteristics, because they do not feature an exponential decay with wavelength. In contrast, the ferulic acid absorption spectra have a typical molecular-band appearance. Still, there is no reason to believe that the chromophores and fluorophores of humic substances should coincide. The wavelengths of the absorption maxima of the three species of ferulic acid, located above 250 nm, follow the order $HFA^- < H_2FA < FA^{2-}$, which can be rationalised in the same way (HOMO and LUMO energies) already seen in the case of fluorescence emission.

Supplementary Material. The associated SM file contains: calculated absolute and relative electronic and free energies; FA species distribution diagram; simulated absorption spectra; data on electronic transitions, graphical representation of frontier molecular orbitals (HOMO and LUMO); relevant group charges; molecular structures of S_0 and S_1 states; maps of electrostatic potentials; EEM spectra of SRHA; excitation spectra of both FA and SRHA.

Acknowledgments. This work was supported by Università di Torino (Local Funding 2017).

References

[1] J. Gerke, Concepts and misconceptions of humic substances as the stable part of soil organic matter: A review, Agronomy 8 (2018) article n. 76.

[2] E. Lipczynska-Kochany, Effect of climate change on humic substances and associated impacts on the quality of surface water and groundwater: A review, Sci. Total Environ. 640-641 (2018) 1548–1565.

[3] E. R. Graber, Y. Rudich, Atmospheric HULIS: How humic-like are they? A comprehensive and critical review, Atmos. Chem. Phys. 6 (2006) 729–753.

[4] J. Wu, Y. Ma, H. Qi, X. Zhao, X. Zhang, X. Xie, Y. Du, Y. Zhao, Z. Wie, R. R.: J. Microbiol. Biotechnol. 6 (2017) 22–27.

[5] A. K. Kiprop, M. C. J. Coumon, E. Pourtier, S. Kimutai, S. Kirui, Synthesis of humic and fulvic acids and their characterization using optical spectroscopy (ATR-FTIR and UV-Visible), Intern. J. Appl. Sci. Technol. 3 (2013) 28–35.

[6] C. S. Uyguner, C. Hellriegel, W. Otto, C. K. Larive, Characterization of humic substances: Implications for trihalomethane formation, Anal. Bioanal. Chem. 378 (2004) 1579–1586.

[7] A. Piccolo, The supramolecular structure of humic substances, Soil Sci. 166 (2001) 810–832.

[8] G. N. Fedotov, S. A. Shoba, On the nature of humic substances, Eurasian Soil Sci. 48 (2015) 1292–1299.

[9] G. E. Schaumann, Soil organic matter beyond molecular structure Part I: Macromolecular and supramolecular characteristics, J. Plant Nutr. Soil Sci. 169 (2006) 145–156.

[10] J. J. Mobed, S. L. Hemmingsen, J. L. Autry, L. B. McGown, Fluorescence characterization of IHSS humic substances: Total luminescence spectra with absorbance correction. Environ. Sci. Technol. 30 (1996) 3061–3065.

[11] P. G. Coble, Characterization of marine and terrestrial DOM in seawater using excitation-emission matrix spectroscopy, Mar. Chem. 51 (1996) 325–346.

[12] B. J. H. Matthews, A. C. Jones, N. K. Theodorou, A. W. Tudhope, Excitation-emission-matrix fluorescence spectroscopy applied to humic acid bands in coral reefs, Mar. Chem. 55 (1996) 317–332.

[13] C. H. Santos, G. Nicolodelli, R. A. Romano, A. M. Tadini, P. R. Villas-Boas, C. R. Montes, S. Mounier, D. M. B. P. Milori, Structure of humic substances from some regions of the Amazon assessed coupling 3D fluorescence spectroscopy and CP/PARAFAC, J. Braz. Chem. Soc. 26 (2015) 1136–1142.

[14] A. Stubbins, J.-F. Lapierre, M. Berggren, Y. T. Prairie, T. Dittmar, P. A. del Giorgio, What's in an EEM? Molecular signatures associated with dissolved organic fluorescence in Boreal Canada, Environ. Sci. Technol. 48 (2014) 10598–10606.

[15] M. Bieroza, A. Baker, J. Bridgemann, New data mining and calibration approaches to the assessment of water treatment efficiency, Adv. Eng. Soft. 44 (2012) 126–135.

[16] K. R. Murphy, S. A. Timko, M. Gonsior, L. C. Powers, U. J. Wünsch, C. A. Stedmon, Photochemistry illuminates ubiquitous organic matter fluorescence spectra, Environ. Sci. Technol. 52 (2018) 11243–11250.

[17] J. P. Aguer, C. Richard, Photochemical behaviour of humic acid synthesized from phenol, J. Photochem. Photobiol. A: Chem. 84 (1994) 69–73.

[18] A. Bianco, M. Minella, E. De Laurentiis, V. Maurino, C. Minero, D. Vione, Photochemical generation of photoactive compounds with fulvic-like and humic-like fluorescence in aqueous solution, Chemosphere 111 (2014) 529–536.

[19] Y. Li, D. D. Huang, H. Y. Cheung, A. K. Y. Lee, C. K. Chan, Aqueous-phase photochemical oxidation and direct photolysis of vanillin – A model compound of methoxy phenols from biomass burning. Atmos. Chem. Phys. 14 (2014) 2871–2885.

[20] D. D. Huang, Q. Zhang, H. H. Y.Cheung, L. Yu, S. Zhou, C. Anastasio, J. D. Smith, C. K. Chan, Formation and evolution of aqSOA from aqueous-phase reactions of phenolic carbonyls: comparison between ammonium sulfate and ammonium nitrate solutions. Environ. Sci. Technol. 52 (2018) 9215–9224.

[21] F. Barsotti, G. Ghigo, D. Vione, Computational assessment of the fluorescence emission of phenol oligomers: A possible insight into the fluorescence properties of humic-like substances (HULIS). J. Photochem. Photobiol. A: Chem. 315 (2016) 87–93.

[22] F. Barsotti, G. Ghigo, S. Berto, D. Vione, The nature of the light absorption and emission transitions of 4-hydroxybenzophenone in different solvents. A combined computational and experimental study. Photochem. Photobiol. Sci. 16 (2017) 527–538.

[23] G. Ghigo, S. Berto, M. Minella, D. Vione, E. Alladio, V. M. Nurchi, J. Lachowicz, P. G. Daniele, New insights into the protogenic and spectroscopic properties of commercial tannic acid: The role of gallic acid impurities. New J. Chem. 42 (2018) 7703–7712.

[24] S. Berto, E. De Laurentiis, C. Scapuzzi, E. Chiavazza, I. Corazzari, F. Turci, M. Minella, R. Buscaino, P. G. Daniele, D. Vione, Phototransformation of L-tryptophan and formation of humic substances in water, Environ. Chem. Lett. 16 (2018) 1035–1041.

[25] D. M. de Oliveira, A. Finger-Teixeira, T. R. Mota, V. H. Salvador, F. C. Moreira-Vilar, H. B. Molinari, R. A. Mitchell, R. Marchiosi, O. Ferrarese-Filho, W. D. dos Santos, Ferulic acid: a key component in grass lignocellulose recalcitrance to hydrolysis, Plant Biotechnol. J. 13 (2015) 1224–1232.

[26] L. J. Jönsson, C. Martín, Pretreatment of lignocellulose: Formation of inhibitory by-products and strategies for minimizing their effects, Biores. Technol. 199 (2016) 103–112.

[27] S. Meyer, A. Cartelat, I. Moya, Z. G. Cerovic, UV-induced blue-green and far-red fluorescence along wheat leaves: A potential signature of leaf ageing. J. Exp. Bot. 54 (2003) 757–769.

[28] U. Wünsch, K. Murphy, C. A. Stedmon, Fluorescence quantum yields of natural organic matter and organic compounds: Implications for the fluorescence-based interpretation of organic matter composition. Front. Mar. Sci. 2 (2015) article n. 98.

[29] S. E. Braslavsky, Glossary of terms used in photochemistry, 3rd edition. Pure Appl. Chem. 79 (2007) 293-465.

[30] F. Jensen, Introduction to Computational Chemistry, John Wiley & Sons, NY, 1999, ISBN 0-471-98425-98426.

[31] R.G. Parr, W. Yang, Density Functional Theory of Atoms and Molecules, Oxford University Press, 1989.

[32] W. Kohn, A.D. Becke, R.G. Parr, Density functional theory of electronic structure, J. Phys. Chem. 100 (1996) 12974–12980.

[33] A. V. Marenich, C. J. Cramer, D. G. Truhlar, Universal Solvation Model Based on Solute Electron Density and on a Continuum Model of the Solvent Defined by the Bulk Dielectric Constant and Atomic Surface Tensions, J. Chem. Phys. B 113 (2009) 6378–6396.

[34] A. V. Marenich, C. J. Cramer, D. G. Truhlar, Performance of SM6, SM8, and SMD on the SAMPL1 Test Set for the Prediction of Small-Molecule Solvation Free Energies, J. Chem. Phys. B 113 (2009) 4538–4543.

[35] R. Bauernschmitt, R. Ahlrichs, Treatment of electronic excitations within the adiabatic approximation of time dependent density functional theory, Chem. Phys. Lett. 256 (1996) 454–464.

[36] A. Dreuw, M. Head-Gordon, Single-reference ab initio methods for the calculation of excited states of large molecules, Chem. Rev. 105 (2005) 4009–4037.

[37] D. Jacquemin, V. Wathelet, E. A. Perpète, C. Adamo, Extensive TD-DFT benchmark: Singlet-excited states of organic molecules, J. Chem. Theory Comput. 5 (2009) 2420–2435.

[38] A. D. Laurent, D. Jacquemin, TD-DFT Benchmarks: A Review, Int. J. Quantum Chem. 113, (2013) 2019–2039.

[39] A. Charaf-Eddin, A. Planchat, B. Mennucci, C. Adamo, D. Jacquemin, Choosing a functional for computing absorption and fluorescence band shapes with TD-DFT, J. Chem. Theory Comput. 9 (2013) 2749–2760.

[40] Peter and Julio de Paula Atkins. Physical Chemistry for the Life Sciences. 2006. New York, NY: W.H. Freeman and Company. p. 563–564.

[41] J. P. Perdew, K. Burke, M. Ernzerhof, Generalized gradient approximation made simple, Phys. Rev. Lett. 77 (1996), 3865–3868.

[42] J. P. Perdew, K. Burke, M. Ernzerhof, Errata: Generalized gradient approximation made simple, Phys. Rev. Lett. 78 (1997), 1396.

[43] C. Adamo, V. Barone, Toward reliable density functional methods without adjustable parameters: The PBE0 model, J. Chem. Phys. 110 (1999) 6158-6168.

[44] Self-consistent molecular orbital methods. XX. A basis set for correlated wave functions, J. Chem. Phys. 72 (1980), 650–654.

[45] T. Clark, J. Chandrasekhar, G. W. Spitznagel, P. V. R. Schleyer, Efficient diffuse function-augmented basis sets for anion calculations. III. The 3-21+G basis set for first-row elements, Li–F, J. Comput. Chem. 4 (1983) 294–301.

[46] T. Matsui, T. Baba, K. Kamiyad, Y. Shigetab, An accurate density functional theory based estimation of pKa values of polar residues combined with experimental data: from amino acids to minimal proteins, Phys. Chem. Chem. Phys. 14 (2012) 4181–4187.

[47] M. J. Frisch, G. W. Trucks, H. B. Schlegel, G. E. Scuseria, M. A. Robb, J. R. Cheeseman, G. Scalmani, V. Barone, B. Mennucci, G. A. Petersson, H. Nakatsuji, M. Caricato, X. Li, H. P. Hratchian, A. F. Izmaylov, J. Bloino, G. Zheng, J. L. Sonnenberg, M. Hada, M. Ehara, K. Toyota, R. Fukuda, J. Hasegawa, M. Ishida, T. Nakajima, Y. Honda, O. Kitao, H. Nakai, T. Vreven, J. A. Montgomery Jr., J. E. Peralta, F. Ogliaro, M. Bearpark, J. J. Heyd, E. Brothers, K. N. Kudin, V. N. Staroverov, R. Kobayashi, J. Normand, K. Raghavachari, A. Rendell, J. C. Burant, S. S. Iyengar, J. Tomasi, M. Cossi, N. Rega, J. M. Millam, M. Klene, J. E. Knox, J. B. Cross, V. Bakken, C. Adamo, J. Jaramillo, R. Gomperts, R. E. Stratmann, O. Yazyev, A. J. Austin, R. Cammi, C. Pomelli, J. W. Ochterski, R. L. Martin, K. Morokuma, V. G. Zakrzewski, G. A. Voth, P. Salvador, J. J. Dannenberg, S. Dapprich, A. D. Daniels, Ö. Farkas, J. B. Foresman, J. V. Ortiz, J. Cioslowski, D. J. Fox, Gaussian 09, Gaussian, Inc., Wallingford, CT, 2009.

[48] G. Schaftenaar, J. H. Noordik, Molden: a pre- and post-processing program for molecular and electronic structures, J. Computer-Aided Mol. Des. 14 (2000) 123–134.

[49] F. Borges, J. L. F. C. Lima, I. Pinto, S. Reis, C. Siquet, Application of a potentiometric system with data-analysis computer programs to the quantification of metal-chelating activity of two natural antioxidants: Caffeic acid and ferulic acid, Helv. Chim. Acta, 8 (2003) 3081–3087.

[50] A. Casale, P. G. Daniele, A. De Robertis, S. Sammartano, Ionic strength dependence of formation constants. Part XI. An analysis of literature data on carboxylate ligand complexes, Ann. Chim. (Rome) 78 (1988) 249–260.

[51] R. Del Vecchio, T. M. Schendorf, N. V. Blough, Contribution of quinones and ketones/aldehydes to the optical properties of humic substances (HS) and chromophoric dissolved organic matter (CDOM), Environ. Sci. Technol. 51 (2017) 13624-13632.

[52] G. McKay, J. A. Korak, P. R. Erickson, D. E. Latch, K. McNeill, F. L. Rosario-Ortiz, The case against charge transfer interactions in dissolved organic matter photophysics, Environ. Sci. Technol. 52 (2018) 406-414.

[53] F. W. J. Teale, The ultraviolet fluorescence of proteins in neutral solution, Biochem. J. 76 (1960) 381-388.

[54] F. Barsotti, M. Brigante, M. Sarakha, V. Maurino, C. Minero, D. Vione, Photochemical processes induced by the irradiation of 4-hydroxybenzophenone in different solvents, Photochem. Photobiol. Sci. 14 (2015) 2087-2096.

[55] D. Vione, A. Albinet, F. Barsotti, M. Mekic, B. Jiang, C. Minero, M. Brigante, S. Gligorovski, Formation of substances with humic-like fluorescence properties, upon photoinduced oligomerization of typical phenolic compounds emitted by biomass burning, Atmos. Environ. 206 (2019) 197-207.

[56] M. Kasha, Characterization of electronic transitions in complex molecules, Discuss. Faraday Soc. 9 (1950) 14–19.

[57] F. Crea, C. De Stefano, A. Gianguzza, A. Pettignano, D. Piazzese, S. Sammartano, Acid–base properties of synthetic and natural polyelectrolytes: Experimental results and models for the dependence on different aqueous media, J. Chem. Eng. Data 54 (2009) 589-605.